Hindawi Publishing Corporation
Journal of Atomic and Molecular Physics
Volume 2014, Article ID 431592, 11 pages
http://dx.doi.org/10.1155/2014/431592

Research Article

A Model of Calculating Radiative Opacities of Hot Dense Plasmas Based on the Density-Functional Theory

Shuji Kiyokawa

Department of Physics, Faculty of Science, Nara Women's University, Kitauoyanishi-machi, Nara 630-8506, Japan

Correspondence should be addressed to Shuji Kiyokawa; sk@cc.nara-wu.ac.jp

Received 19 February 2014; Revised 14 July 2014; Accepted 15 July 2014; Published 2 September 2014

Academic Editor: George C. King

We determine the radiative opacity of plasmas in a local thermal equilibrium (LTE) by time-dependent density-functional theory (TDDFT) including autoionization resonances, where the photoabsorption cross section is calculated for an ion embedded in the plasma using the detailed configuration accounting (DCA) method. The abundance of ion with integer occupation numbers is determined by means of the finite temperature density-functional theory (FTDFT). For an Al plasma of temperature $T = 20\,\text{eV}$ and density $0.01\,\text{g/cm}^3$, we show the opacity and the photoabsorption cross section of b-f and b-b transitions with Doppler and Stark width, and also show a result that the Planck and Rosseland mean opacities are 28,348 cm^2/g and 4,279 cm^2/g, respectively.

1. Introduction

For investigation of hot dense plasmas, the density-functional theory has been used to calculate their atomic properties and has provided reliable data such as electronic structure, equation of state (EOS), and opacity [1–7]. Particularly, the study of radiative properties of inertial confinement plasmas, interior of stars, and so on is important and theoretically great interest for the reason that the thermal properties and the electronic ones of plasmas are closely correlated with each other.

The most popular model for the hot dense plasmas is the average atom (AA) model [5, 8–11], and it has been employed vigorously to study the opacity [12] and so on. However, as an actual LTE plasma is composed of various ions in different excited states and charge states; the spectral structure of LTE plasma is very complex because of the enormous number of transition lines. The method of the supertransition array (STA) [7, 12–14] has been used to analyze such a complex line spectrum of an ion in a LTE plasma.

For the dense plasmas, autoionization is an intrinsically crucial atomic process and is important for treatments of plasma opacity, but the autoionization and the ion-ion pair distribution function are not treated in calculations of the opacities by STA. One of methods of calculating the autoionization in the dense plasmas is the time-dependent density-functional theory which is treated the autoionization resonance as the dynamical linear response of electronic system.

To calculate the opacity of plasmas, we have considered the time-dependent density-functional theory (TDDFT) to treat the photoabsorption cross section of plasmas, where the autoionization process is included without using any other code [15].

In this method, LTE plasmas are treated by finite temperature density-functional theory (FTDFT) [16, 17] and all the calculations are carried out within the framework of density-functional theory (DFT). The method is fast and stable for the numerical calculation of autoionization resonance. The resonance energy point obtained by our method is found to be equal to the difference of two related orbital energies shifted by an amount due to the relaxation effects of electrons in the time-dependent external electric field.

In Section 2, we review the formulation of LTE plasmas by FTDFT [16, 17] in brief. In Section 3, a model of the calculation of the photoabsorption cross section of LTE plasmas is shown by TDDFT, where ions in the plasmas are "real ion" with integer numbers of bound electrons. The opacity of an Al plasma is shown in Section 4, and we compare our results with other experimental and theoretical results. We conclude with a short summary in Section 5.

2. A Self-Consistent Model of Plasmas: FTDFT

Int this section, we review the finite temperature density functional theory for plasmas (FTDFT) [15, 18–20], briefly. We consider a plasma containing N_n nuclei of nuclear charge Z_a and $N_n Z_a$ electrons in a volume V_{sys}. The system is in thermal equilibrium with temperature T (in energy unit).

The Hamiltonian of the system is as follows (hereafter, we use atomic units):

$$H_{\text{sys}} = \sum_{j=1}^{N_n} \frac{\mathbf{P}_j^2}{2M} + \sum_{i>j} \frac{(Z_a)^2}{|\mathbf{R}_i - \mathbf{R}_j|} + H_e,$$
$$H_e = \sum_j \left(-\frac{1}{2} \frac{\partial^2}{\partial \mathbf{r}_j^2} \right) + \sum_{i>j} \frac{1}{|\mathbf{r}_i - \mathbf{r}_j|} - \sum_{i,j} \frac{Z_a}{|\mathbf{R}_i - \mathbf{r}_j|}, \tag{1}$$

where M, $\mathbf{P}$ are nuclear mass, momentum of a nucleus, respectively, and $\mathbf{R}$ and $\mathbf{r}$ denote the positions of nucleus and electron, respectively. We assumed here that the nuclear motion can be treated classically, while the electron subsystem obeys the quantum mechanics. We also assumed the plasma consists of average ions and uniform continuum electrons, where the electronic structure of the average ion is determined by the Kohn-Sham equation as follows:

$$\frac{1}{r^2} \frac{d}{dr} \left(r^2 \frac{dR_{n\ell}}{dr} \right) + 2 \left(\varepsilon_{n\ell} - v_{\text{eff}}(r) - \frac{\ell(\ell+1)}{2r^2} \right) R_{n\ell} = 0$$
$$R_{n\ell}(\infty) = 0, \tag{2}$$

where n, ℓ are principle quantum number and angular momentum of electron and $v_{\text{eff}}(r)$ is the effective potential at finite temperature including the exchange-correlation potential:

$$v_{\text{eff}}(r) = -\frac{Z_a}{r} + \int \frac{\overline{\rho_b}(r') - Q_s(r')}{|\mathbf{r} - \mathbf{r}'|} d\mathbf{r}'$$
$$+ v_{xc}\left[\overline{\rho_b}(r) + \rho_c\right] - v_{xc}\left[\rho_c\right], \tag{3}$$

where ρ_c is the continuum electron density,

$$\rho_c = \frac{\sqrt{2}}{\pi^2} \int_0^\infty \frac{\sqrt{\varepsilon}}{e^{\beta(\varepsilon - \mu_e)} + 1} d\varepsilon, \tag{4}$$

and $\overline{\rho_b}(\mathbf{r})$ is the bound electron density of the average ion,

$$\overline{\rho_b}(r) = \frac{1}{4\pi} \sum_{n\ell} \frac{2(2\ell+1)}{\exp\left[\beta(\varepsilon_{n\ell} - \mu_e)\right] + 1} R_{n\ell}(r)^2. \tag{5}$$

The chemical potential μ_e of electron subsystem is determined by ensuring the charge neutrality of the system

$$Z_a = \sum_{n\ell} \frac{2(2\ell+1)}{\exp\left[\beta(\varepsilon_{n\ell} - \mu_e)\right] + 1} + \frac{\rho_c}{\rho_{\text{ion}}}, \tag{6}$$

where ρ_{ion} is the ion density of the plasma. The function $Q_s(\mathbf{r})$ in (3) is the charge density, composed of three parts

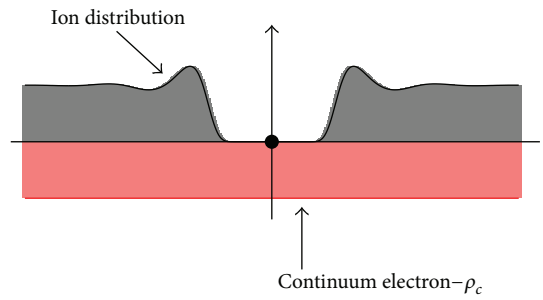

Figure 1: The image of the charge density $Q_s(r)$ of (7). In this figure, the black circle • shows a nucleus located at the origin of the coordinate system. "Ion distribution" means the sum of the first and second terms of the right-hand side in (7).

(Figure 1): (i) the charge density $Z_a \rho_{\text{ion}} g_{ii}(\mathbf{r})$ of the other nucleus crowded around the ion located at the origin of the coordinate system, (ii) the bound electrons density of these nucleus, and (iii) the uniform background electron charge density $-\rho_c$, as follows:

$$Q_s(r) = Z_a \rho_{\text{ion}} g_{ii}(\mathbf{r}) - \rho_{\text{ion}} \int \overline{\rho_b}(\mathbf{r} - \mathbf{r}') g_{ii}(\mathbf{r}') d\mathbf{r}' - \rho_c. \tag{7}$$

The function $g_{ii}(r)$ is the radial distribution function for the average ion.

The radial distribution function $g_{ii}(r)$ is obtained by hypernetted chain (HNC) approximation [21] as follows:

$$\log\left[g_{ii}(r)\right] = -\beta\phi(r) + \rho_{\text{ion}} \int C\left(|\mathbf{r} - \mathbf{r}'|\right) G_{ii}(\mathbf{r}') d\mathbf{r}', \tag{8}$$

where functions $G_{ii}(\mathbf{r}) \equiv g_{ii} - 1$ and $C(\mathbf{r})$ are the direct correlation function, and these functions must satisfy the next Ornstein-Zernike's relation:

$$G_{ii}(\mathbf{r}) = C(\mathbf{r}) + \rho_{\text{ion}} \int C\left(|\mathbf{r} - \mathbf{r}'|\right) G_{ii}(\mathbf{r}') d\mathbf{r}'. \tag{9}$$

The function $\phi(r)$ in (8), the effective interatomic potential, is the electrostatic interaction between two average ions separated distance $\mathbf{R}$, and is approximately calculated as follows:

$$\phi(r) = \frac{Z_a^2}{r} - 2\int \frac{Z_a \overline{\rho_b}(r')}{|\mathbf{r} - \mathbf{r}'|} d\mathbf{r}' + \iint \frac{\overline{\rho_b}(r_1)\overline{\rho_b}(r_2)}{|\mathbf{r} + \mathbf{r}_1 - \mathbf{r}_2|} d\mathbf{r}_1 d\mathbf{r}_2, \tag{10}$$

where the polarization of continuum electrons is neglected.

3. A Modeling of Absorption Cross Section: TDDFT

In our previous theory [15] of the photoabsorption cross section for plasmas by means of time-dependent density functional theory (TDDFT) [22–25], we employed the average ion model of calculating the electronic structure of ions in the plasma, where all ions have the same electronic structure. In this section, we extend our previous formula for the photoabsorption cross section to apply in the case of the photoabsorption by real ions in the plasma.

3.1. Probability of Existence of an Ion. When plasmas are in LTE, electronic state of ion in the plasma will be in every possible state, that is, the number of bound electrons in an orbital of the ion fluctuates around the average value. The electronic configuration of average atom model is a virtual image obtained by a time average for these deviated states. In our presented model, these average values of occupation are calculated by means of FTDFT as mentioned in Section 2.

The relaxation time τ of this fluctuation will estimate roughly by the mean time between two-electron or ion-electron collisions. For the spatial distribution of surrounding an ion (given by (8)), the relaxation time of its fluctuation will roughly be equal to the mean collision time between ions, and it is very large compared to the electron collision time. On the other hand, the photoabsorption occurs in very short time compared with that fluctuation time τ. Therefore, electronic state of ions going to absorb photon is in one of deviated states from the average atom, and this ion will be in electric field caused by deviation of spatial distribution of ions. Then, we must prepare a deviated electronic state, that is, a electronic configuration with integer occupation for an initial state of ion, but we here assume that the ion spatial distribution is given by (8) without fluctuation, and other ions around an ion at origin are replaced with average atoms obtained by FTDFT (so-called the constant density method [12]).

In the calculation of the opacity of LTE plasmas, it is necessary to know the probability distribution of excited electronic state of an ion with integer occupation, where the plasma effects (the ionization potential depression (IPD [26]), pressure ionization, etc.) must be correctly taken into account. To consider this probability distribution, we calculate the energy of an ion with integer occupation numbers of bound electrons embedded in the plasma, where the electrostatic potential surrounding that ion is determined by continuum electrons, the spatial distribution of neighboring ions, and their electronic structure. Therefore, the IPD is included in calculation of opacity.

For a given electron configuration

$$(1s)^{q_1}(2s)^{q_2}(2p)^{q_3}(3s)^{q_4}(3p)^{q_5}(3d)^{q_6}\cdots \tag{11}$$

with integer occupation numbers $(q_1, q_2, q_3, q_4, \ldots)$, there are many terms with different energies in general; however, we assume that the average energy of an electron configuration of an ion [27] can be calculated as follows:

$$E_{\{\mathbf{q}\}} = \sum_i q_i\varepsilon_i - \frac{1}{2}\iint \frac{\rho_{\{\mathbf{q}\}}(r)\,\rho_{\{\mathbf{q}\}}(r')}{|\mathbf{r}-\mathbf{r}'|}d\mathbf{r}\,d\mathbf{r}' - \frac{3}{4}\int \rho_{\{\mathbf{q}\}}(r)\,v_x\left[\rho_{\{\mathbf{q}\}}(r)\right]d\mathbf{r}, \tag{12}$$

where $v_x[\rho_{\{\mathbf{q}\}}(r)]$ and $\rho_{\{\mathbf{q}\}}(r)$ are the exchange potential and the bound electron density, respectively;

$$v_x\left[\rho_{\{\mathbf{q}\}}(r)\right] = -\left(\frac{3}{\pi}\rho_{\{\mathbf{q}\}}(r)\right)^{1/3}, \tag{13}$$

$$\rho_{\{\mathbf{q}\}}(r) = \frac{1}{4\pi}\sum_i q_i R_i(r)^2, \tag{14}$$

$\{\mathbf{q}\}$ denotes a set of occupation numbers $(q_1, q_2, q_3, \ldots)$, and ε_i and R_i are the bound electron energy and radial wave function of orbital i obtained by the Kohn-Sham equation which is obtained by replacing the potential $v_{\text{eff}}(r)$ in (2) by the following potential:

$$V_{\{\mathbf{q}\}}(r) = -\frac{Z_a}{r} + \int \frac{\rho_{\{\mathbf{q}\}}(\mathbf{r}') - Q_s(\mathbf{r}')}{|\mathbf{r}-\mathbf{r}'|}d\mathbf{r}' + v_x\left[\rho_{\{\mathbf{q}\}}(r)\right]. \tag{15}$$

The probability $P_{\{\mathbf{q}\}}$ of existence for the ion (nuclear charge Z_a) with an electronic configuration of integer occupation numbers $\{\mathbf{q}\}$ is given as the change in the total energy of the ion. The probability $P_{\{\mathbf{q}\}}$ of existence for the ion with an electron configuration $\{\mathbf{q}\}$ is

$$P_{\{\mathbf{q}\}} = \frac{1}{Z_G^{\text{ion}}}\prod_i \binom{g_i}{q_i}\exp\left[-\beta\left(E_{\{\mathbf{q}\}} - \mu_e\sum_i q_i\right)\right], \tag{16}$$

where Z_G^{ion} is a normalization factor, ℓ_i is the angular momentum, and $g_i = 2(2\ell_i + 1)$ is the maximum occupation number of the orbital i [15].

3.2. Photoabsorption Cross Section. We now discuss the photoresponse of an ion in plasmas to a frequency-dependent external field. The electronic configuration of this ion is assumed to be $(1s)^{q_1}2s^{q_2}(2p)^{q_3}(3s)^{q_4}\cdots$. If the incident photon energy ω (in atomic units) is in the vicinity of the difference between two orbital energies $\varepsilon_{n_i\ell_i}$ and $\varepsilon_{n_f\ell_f}$ ($|\ell_i - \ell_f| = 1$), that is, $\omega \sim \varepsilon_{n_f\ell_f} - \varepsilon_{n_i\ell_i}$ with $\varepsilon_{n_f\ell_f} - \varepsilon_{n_i\ell_i} > |\varepsilon_{n_f\ell_f}|$, one of the $(n_f\ell_f)$ electrons can attain an energy above the ionization energy via the following successive excitation processes:

$$(n_i\ell_i)^{q_i}(n_f\ell_f)^{q_f} \longrightarrow (n_i\ell_i)^{q_i-1}(n_f\ell_f)^{q_f+1} \longrightarrow (n_i\ell_i)^{q_i}(n_f\ell_f)^{q_f-1}(\varepsilon\ell)^1; \tag{17}$$

consequently, the $(n_f\ell_f)$ electron can be ejected. Another process can coincide with this process; that is, one of the $(n_f\ell_f)$ electrons can directly absorb the photon energy ω:

$$(n_i\ell_i)^{q_i}(n_f\ell_f)^{q_f} \longrightarrow (n_i\ell_i)^{q_i}(n_f\ell_f)^{q_f-1}(\varepsilon\ell)^1. \tag{18}$$

These two processes compete with each other; namely, a channel mixing occurs, and consequently, the Fano profile appears on the photoabsorption cross section. If the energies of the $\varepsilon_{n_i\ell_i}$ and the $\varepsilon_{n_f\ell_f}$ do not satisfy the condition $\varepsilon_{n_f\ell_f} - \varepsilon_{n_i\ell_i} > |\varepsilon_{n_f\ell_f}|$, the channel mixing cannot occur in our calculation, but a direct bound-bound transition

$$(n_i\ell_i)^{q_i}(n_f\ell_f)^{q_f} \longrightarrow (n_i\ell_i)^{q_i-1}(n_f\ell_f)^{q_f+1} \tag{19}$$

can occur if the photon energy satisfies the resonance condition $\hbar\omega = \varepsilon_{n_f\ell_f} - \varepsilon_{n_i\ell_i}$. To investigate the above processes, we study how the electrons respond to a frequency-dependent external field.

3.2.1. Photoabsorption Cross Section of an Ion: $\sigma(\omega : \{\mathbf{q}\})$. In previous theory [15], we considered only bound-free contribution to the calculation of the photoabsorption cross section, but here we extend the theory to include the bound-bound absorption.

We assume that the frequency-dependent external electric field is of magnitude E_0 directed along the z-axis. The interaction between this field and the electrons of an ion is $\int \rho_b(\mathbf{r})\phi_{\text{ext}}(\mathbf{r},\omega)e^{i\omega t}d\mathbf{r}$, where $\rho_b(\mathbf{r})$ is the bound electron density, and

$$\begin{aligned}\phi_{\text{ext}}(\mathbf{r},\omega) &= E_0\sqrt{\frac{4\pi}{3}}rY_{10}(\hat{\mathbf{r}}) \\ &\equiv E_0\phi_\omega^{\text{ext}}(r)\,Y_{10}(\hat{\mathbf{r}}).\end{aligned} \tag{20}$$

The induced charge density $\delta\rho_\omega(r)$ in the presence of the external field $\phi_\omega^{\text{ext}}(r)$ is calculated by means of the single particle response function $\chi_\omega^0(r,r')$ [22–24] as follows:

$$\delta\rho_\omega(r) = \int_0^\infty \chi_\omega^0(r,r')\,\phi_\omega^{\text{scf}}(r')\,r'^2dr', \tag{21}$$

where $\phi_\omega^{\text{scf}}(r)$ is the self-consistent field produced by the photoresponse of the electrons. The self-consistent field $\phi_\omega^{\text{scf}}(r)$ is determined by the following relations:

$$\phi_\omega^{\text{scf}}(r) = \phi_\omega^{\text{ext}}(r) + \phi_\omega^{\text{ind}}(r), \tag{22}$$

where $\phi_\omega^{\text{ind}}(r)$ is the frequency-dependent induced potential

$$\begin{aligned}\phi_\omega^{\text{ind}}(r) &= \int_0^\infty \left(\frac{4\pi}{3}\frac{r_<}{r_>^2} + \left.\frac{\delta v_x[\rho_{\{\mathbf{q}\}}(r)]}{\delta\rho}\right|_{\rho(\mathbf{r}')}\frac{\delta(r-r')}{r'^2}\right) \\ &\quad\times\delta\rho_\omega(r')\,r'^2dr' \\ &\equiv \int_0^\infty K(r,r')\,\delta\rho_\omega(r')\,dr'.\end{aligned} \tag{23}$$

In the above equation, the 2nd term in the integrand is a functional derivative of the exchange potential $v_x[\rho(r)]$. From (13), the functional derivative of exchange potential $v_x[\rho(\mathbf{r})]$ is in proportion to $\rho(\mathbf{r})^{-2/3}$

$$\begin{aligned}&\int \left.\frac{\delta v_x[\rho]}{\delta\rho}\right|_{\rho_{\{\mathbf{q}\}}(\mathbf{r}')}\frac{\delta(r-r')}{r'^2}\delta\rho_\omega(r')\,r'^2dr' \\ &\quad= \frac{v_x[\rho_{\{\mathbf{q}\}}(r)]}{3\rho_{\{\mathbf{q}\}}(r)}\delta\rho_\omega(r).\end{aligned} \tag{24}$$

When a photon energy ω is in the vicinity of the energy deference of optically allowed two- bound states $n_i\ell_i$ and $n_f\ell_f$, namely, $\omega \sim \varepsilon_f - \varepsilon_i \equiv \Delta\varepsilon$, the response function $\chi_\omega^0(r,r')$ in (21) is given as follows:

$$\begin{aligned}\chi_\omega^0(r,r') &\simeq 2f_i(1-f_f)\,C_{\ell_i\ell_f}\eta_{if}R_{n_i\ell_i}(r)\,R_{n_f\ell_f}(r) \\ &\quad\times R_{n_f\ell_f}(r')\,R_{n_i\ell_i}(r') \\ &\quad+ \sum_{s<s'}{}' 2f_s(1-f_{s'})\,C_{\ell_s\ell_{s'}}\eta_{s,s'}R_s(r)\,R_{s'}(r) \\ &\quad\times R_{s'}(r')\,R_s(r') \\ &\quad- i\pi\sum_s\sum_{\ell=\ell_s\pm1} 2f_s(1-f(\varepsilon_s+\omega))\,C_{\ell_s\ell} \\ &\quad\times R_s(r)\,R_{(\varepsilon_s+\omega)\ell}(r)\,R_{(\varepsilon_s+\omega)\ell}(r') \\ &\quad\times R_s(r')\,\theta(\varepsilon_s+\omega),\end{aligned} \tag{25}$$

where $f_s = q_s/[2(2\ell_s+1)]$, $\theta(\varepsilon_s+\omega)$ is the unit step function, and $C_{\ell\ell'}$, $\eta_{n\ell,n'\ell'}$ are given as

$$C_{\ell\ell'} = \begin{cases}\dfrac{\ell+\ell'+1}{8\pi} & \text{for } |\ell-\ell'| = 1 \\ 0 & \text{for } |\ell-\ell'| \neq 1,\end{cases} \tag{26}$$

$$\eta_{if} = \frac{1}{\omega-\Delta\varepsilon+i\delta} - \frac{1}{\omega+\Delta\varepsilon+i\delta}, \quad \Delta\varepsilon = \varepsilon_f - \varepsilon_i. \tag{27}$$

In (25), summations for s are over only occupied orbitals, as distinct from $\chi_\omega^0(r,r')$ for finite temperature where summation is over all occupied and unoccupied orbitals [15]. In the second term on the right-hand side of (25), the double summation runs over all bound states on the condition $\varepsilon_s < \varepsilon_{s'}$, and the prime denotes the omission of two bound states $(n_i\ell_i)$ and $(n_f\ell_f)$.

In (27), the factor δ is a infinitesimal positive quantity. The factor $\eta_{s,s'}$ in this term is real value and given as follows:

$$\eta_{s,s'} = \frac{1}{\varepsilon_s-\varepsilon_{s'}+\omega} - \frac{1}{\varepsilon_{s'}-\varepsilon_s+\omega}. \tag{28}$$

The $R_{E\ell}(r)$ in (25) is the radial wave function of a photoionized electron of positive energy E and angular momentum ℓ, which is obtained by solving the Kohn-Sham equation.

3.2.2. Bound-Free Absorption. We rewrite the first term and the sum in the second term of (25) to a single sum as follows:

$$\sum_{k=0,1,2,\ldots}^{k_{\max}} c_k\eta_k U_k(r)\,U_k(r'), \tag{29}$$

where the term of $k = 0$ in above sum corresponds to the first term of (25) and the factors c_0, η_0 and the function $U_0(r)$ are given as follows:

$$c_0 = 2f_i\left(1 - f_f\right)C_{\ell_i\ell_f},$$
$$\eta_0 = \eta_{if}, \tag{30}$$
$$U_0(r) = R_{n_i\ell_i}(r)\,R_{n_f\ell_f}(r).$$

The other terms ($k = 1, 2, \ldots$) in the sum equation (29) correspond to the nonvanishing terms on the second term of (25), and the factors c_k, η_k and the function $U_k(r)$ are determined by a combination of two bound states as follows:

$$c_k = 2f_s\left(1 - f_{s'}\right)C_{\ell_s\ell_{s'}},$$
$$\eta_k = \eta_{s,s'}, \tag{31}$$
$$U_k(r) = R_s(r)\,R_{s'}(r).$$

Here, we assume that the number of all nonvanishing terms in the second term of (25) is $k_{\max}$.

In similar manner, numbering $k_{\max} + 1$, $k_{\max} + 2, \ldots$ for all nonvanishing terms on the third term of (25), we rewrite it as follows:

$$\sum_{k>k_{\max}} c_k\eta_k U_k(r)\,U_k\left(r'\right), \tag{32}$$

where the factors c_k, η_k and the function $U_k(r)$ are, respectively,

$$c_k = 2f_s\left(1 - f\left(\varepsilon_s + \omega\right)\right)C_{\ell_s\ell}\theta\left(\varepsilon_s + \omega\right),$$
$$\eta_k = -i\pi, \tag{33}$$
$$U_k(r) = R_s(r)\,R_{(\varepsilon_s+\omega)\ell}(r).$$

Then, (25) can be expressed as

$$\chi_\omega^0\left(r, r'\right) = \sum_{k=0} c_k\eta_k U_k(r)\,U_k\left(r'\right). \tag{34}$$

Substituting (34) into (21), we obtain the radial part of the induced electron density $\delta\rho_\omega(r)$ as follows:

$$\delta\rho_\omega(r) = c_0U_0(r)\,a_0 + \sum_{k=1} c_k\eta_k U_k(r)\,a_k, \tag{35}$$

where complex coefficients a_0 and a_k are given as follows:

$$a_0 = \eta_0\int_0^\infty U_0(r)\,\phi_\omega^{\mathrm{scf}}(r)\,r^2dr$$
$$a_k = \int_0^\infty U_k(r)\,\phi_\omega^{\mathrm{scf}}(r)\,r^2dr, \quad k > 0. \tag{36}$$

From (22), (23), and (35), the self-consistent field $\phi_\omega^{\mathrm{scf}}(r)$ satisfies

$$\phi_\omega^{\mathrm{scf}}(r) = \phi_\omega^{\mathrm{ext}}(r) + c_0B_0(r)\,a_0 + \sum_{k=1} c_k\eta_k B_k(r)\,a_k. \tag{37}$$

The function $B_k(r)$ is given by

$$B_k(r) = \int_0^\infty K\left(r, r'\right)U_k\left(r'\right)r'^2dr'. \tag{38}$$

The self-consistent field $\phi_\omega^{\mathrm{scf}}(r)$ is obtained by simultaneously solving (36) and (37). Substituting (37) into (36), we obtain the following relation:

$$\widehat{V}\begin{pmatrix} a_0 \\ a_1 \\ a_2 \\ \vdots \end{pmatrix} = \begin{pmatrix} d_0 \\ d_1 \\ d_2 \\ \vdots \end{pmatrix}, \tag{39}$$

where the factor d_k is

$$d_k = \int_0^\infty U_k(r)\,\phi_\omega^{\mathrm{ext}}(r)\,r^2dr, \tag{40}$$

and $\widehat{V}$ is the matrix given as follows:

$$\begin{pmatrix} \frac{1}{\eta_0} - V_{00} & -\eta_1V_{01} & -\eta_2V_{02} & -\eta_3V_{03} & \cdots \\ -V_{10} & 1 - \eta_1V_{11} & -\eta_2V_{12} & -\eta_3V_{13} & \cdots \\ -V_{20} & -\eta_1V_{21} & 1 - \eta_2V_{22} & -\eta_3V_{23} & \cdots \\ -V_{30} & -\eta_1V_{31} & -\eta_2V_{32} & 1 - \eta_3V_{33} & \cdots \\ \vdots & \vdots & \vdots & \vdots & \ddots \end{pmatrix}. \tag{41}$$

The factor $V_{kk'}$ in the above matrix elements is given as

$$V_{kk'} = c_{k'}\int_0^\infty U_k(r)\,B_{k'}(r)\,r^2dr. \tag{42}$$

The determinant D of the matrix $\widehat{V}$ can be expanded in terms of its cofactors as follows:

$$D = \left(\frac{1}{\eta_0} - V_{00}\right)A + B, \tag{43}$$

where A and B are the determinants obtained from the cofactors of D. $|D|^2$ becomes

$$|D|^2 = |A|^2\left[\left(\frac{\omega^2 - \varepsilon_r^{(2)}(\omega)}{2\Delta\varepsilon}\right)^2 + \left(\lambda + \frac{\omega}{\Delta\varepsilon}\delta\right)^2\right], \tag{44}$$

(the infinitesimal positive quantity δ in η_0 (or η_{if}, (27)) put 0 in previous theory [15]) where $\Delta\varepsilon = \varepsilon_{n_f\ell_f} - \varepsilon_{n_i\ell_i}$, and

$$\varepsilon_r^{(2)}(\omega) \equiv \Delta\varepsilon^2 + 2\Delta\varepsilon\left(V_{00} - \gamma\right) + \delta^2, \tag{45}$$

and $\lambda \equiv \mathrm{Im}(B/A)$, $\gamma \equiv \mathrm{Re}(B/A)$. The value $\varepsilon_r^{(2)}(\omega)$ of (45) may be negative because of the ω dependence of γ, but if it has a positive value, a positive solution of the relation $\omega^2 - \varepsilon_r^{(2)}(\omega) = 0$ in (44) is considered as a resonance energy position ω_r of Fano profile, and this position is approximately given by

$$\omega_r \simeq \lim_{\delta\to 0}\sqrt{\varepsilon_r^{(2)}(\omega)} = \sqrt{\Delta\varepsilon^2 + 2\Delta\varepsilon\left(V_{00} - \gamma\right)}. \tag{46}$$

The complex coefficients a_0 and a_k satisfy the following relations the same as (43):

$$Da_0 = \left(\frac{1}{\eta_0} - V_{00}\right) A + B';$$
$$Da_k = \left(\frac{1}{\eta_0} - V_{00}\right) P_k + Q_k, \tag{47}$$

then, we obtain the following:

$$a_0 = \frac{1}{D}\begin{vmatrix} d_0 & -\eta_1 V_{01} & -\eta_2 V_{02} & \cdots \\ d_1 & 1-\eta_1 V_{11} & -\eta_2 V_{12} & \cdots \\ d_2 & -\eta_1 V_{21} & 1-\eta_2 V_{22} & \cdots \\ \vdots & \vdots & \vdots & \ddots \end{vmatrix} \equiv \frac{G_0}{D},$$
$$a_1 = \frac{1}{D}\begin{vmatrix} \frac{1}{\eta_0} - V_{00} & d_0 & -\eta_2 V_{02} & \cdots \\ -V_{10} & d_1 & -\eta_2 V_{12} & \cdots \\ -V_{20} & d_2 & 1-\eta_2 V_{22} & \cdots \\ \vdots & \vdots & \vdots & \ddots \end{vmatrix} \equiv \frac{G_1}{D}, \tag{48}$$

and the others are obtained in the same way as a_1.

The photoabsorption cross section is calculated as follows [22, 24]:

$$\sigma(\omega : \{\mathbf{q}\}) = -4\pi\alpha\omega \iint \phi_\omega^{\mathrm{scf}*}(r') \left[\operatorname{Im} \chi_\omega^0(r, r')\right] \times \phi_\omega^{\mathrm{scf}}(r) r'^2 r^2 dr' dr,$$
$$= 4\pi\alpha\omega \left(c_0 \frac{|G_0|^2}{|D|^2} \frac{\omega}{\Delta\varepsilon}\delta + \pi \sum_{k>k_{\max}} c_k \frac{|G_k|^2}{|D|^2} \right), \tag{49}$$

where α is the fine structure constant.

When $\lambda \neq 0$, for $\delta \to 0$ in (49), we obtain the bound-free photoabsorption corss section as follows

$$\sigma(\omega : \{\mathbf{q}\}) = 4\pi^2\alpha\omega \sum_{k>k_{\max}} c_k \frac{|G_k|^2}{|D|^2}. \tag{50}$$

The photoabsorption cross section equation (50) is the superposition of the "Fano profile" and "Lorentz profile" [15].

3.2.3. Bound-Bound Absorption. When the photon energy is in the vicinity of the difference of two orbital energies $\varepsilon_{n_i\ell_i}$ and $\varepsilon_{n_f\ell_f}$, but satisfies the condition $\omega < |\varepsilon_i|$ for any other orbital energies, the matrices A and B in (43) become real values, namely, $\lambda = 0$, $c_k = 0$ $(k > k_{\max})$; the cofactors A and B become real values and autoionization resonance does not occur, though an ordinary bound-bound transition $n_i\ell_i \to n_f\ell_f$ may occur. In this case, the second term of the right-hand side of (49) becomes 0, but the limit of the first term as $\delta \to 0$ is a non-zero value. For calculating the first term in (49), we may expand the $\omega^2 - \varepsilon_r^{(2)}(\omega)$ in (44) into power-series, but neglecting terms in high powers of $(\omega - \omega_r)$ as follows:

$$\omega^2 - \varepsilon_r^{(2)}(\omega)$$
$$\simeq \omega_r^2 - \varepsilon_r^{(2)}(\omega_r) + \left[2\omega_r - \frac{d\varepsilon_r^{(2)}(\omega_r)}{d\omega}\right](\omega - \omega_r)$$
$$= \left(2\omega_r + 2\Delta\varepsilon \frac{d\gamma}{d\omega}\right)(\omega - \omega_r)$$
$$\simeq 2\omega_r(\omega - \omega_r). \tag{51}$$

Then $|D|^2$ in (49) becomes

$$|D|^2 = |A|^2 \left[\left(\frac{\omega_r}{\Delta\varepsilon}\right)^2 (\omega - \omega_r)^2 + \left(\frac{\omega}{\Delta\varepsilon}\delta\right)^2\right]. \tag{52}$$

Therefore the 1st term of the right-hand side in (49) is rewritten as follows:

$$c_0 \frac{|G_0|^2}{|D|^2} \frac{\omega}{\Delta\varepsilon}\delta$$
$$= c_0 |G_0|^2 \frac{1}{|A|^2} \frac{\Delta\varepsilon}{\omega_r} \frac{(\omega/\omega_r)\delta}{\left[(\omega - \omega_r)^2 + ((\omega/\omega_r)\delta)^2\right]}; \tag{53}$$

as a result, the photoabsorption cross section for bound-bound is expressed as

$$\lim_{\delta \to 0} \sigma(\omega : \{\mathbf{q}\}) = 4\pi\alpha\omega c_0 |G_0|^2 \lim_{\delta \to 0} \frac{(\omega/\Delta\varepsilon)\delta}{|D|^2}$$
$$\simeq 4\pi^2\alpha c_0 \Delta\varepsilon \frac{|G_0|^2}{|A|^2} \delta(\omega - \omega_r). \tag{54}$$

From (53), we consider the quantity 2δ as the natural line width of the transition $n_f l_f \to n_i l_i$.

The ω_r is the positive solution of the relation $\omega^2 - \varepsilon_r^{(2)}(\omega) = 0$, and it is the energy point of the resonance absorption of this bound–bound transition. As mentioned above, this energy point is shifted from the difference of the energies of two orbitals involved in the photoabsorption, as for the case of autoionization resonance.

The photoabsorption cross section for a plasma is expressed as

$$\sigma(\omega) = \sum_{\mathbf{q}} P_{\{\mathbf{q}\}} \sigma(\omega : \{\mathbf{q}\}), \tag{55}$$

superimposing the photoabsorption cross section $\sigma(\omega : \{\mathbf{q}\})$ for an ion with a configuration $\mathbf{q} = (q_1, q_2, q_3, \ldots)$, where summation is over electronic configurations ready beforehand (detailed configuration accounting (DCA) method).

4. Results and Discussion

For the purpose of demonstrating the usefulness of our model, we show opacities including autoionization resonances of Al plasma. At first, some physical properties of an

Table 1: Orbital energies and mean orbital radii $\langle r \rangle$ of average atom obtained by FTDFT for Al plasma of temperature $T = 20$ eV and density 0.01 g/cm^3. a_{ion} is the ion-sphere radius, in this case, $a_{\text{ion}} = 19.3563$ in a.u.

Orbital	Occupation	Energy [eV]	$\langle r \rangle / a_{\text{ion}}$
1s	1.0000000	−1593.2399450	0.0062490
2s	0.9471505	−185.2130378	0.0307858
2p	0.7507994	−149.5504598	0.0284118
3s	0.0170534	−46.4087164	0.0893144
3p	0.0112252	−37.9267667	0.0944112
3d	0.0065214	−26.9702796	0.0984221
4s	0.0040830	−17.5564467	0.1868533
4p	0.0035343	−14.6586288	0.2001951
4d	0.0029352	−10.9321117	0.2172469
4f	0.0027064	−9.3044024	0.2041051
5s	0.0024418	−7.2412225	0.3263015
5p	0.0022922	−5.9737677	0.3498977
5d	0.0021112	−4.3251798	0.3842115
5f	0.0020295	−3.5337236	0.3796523
5g	0.0019966	−3.2065049	0.3361391
6s	0.0019489	−2.7221846	0.5264264
6p	0.0018911	−2.1186225	0.5678503
6d	0.0018186	−1.3359917	0.6364388
6f	0.0017813	−0.9203438	0.6548017
6g	0.0017597	−0.6762144	0.6174240
7s	0.0017625	−0.7081767	0.8533281

Al plasma of temperature $T = 20$ eV and density 0.01 g/cm^3 are obtained by means of FTDFT as mentioned in Section 2. The chemical potential μ_e of the electron subsystem and the charge state $Z^*(= Z_a - \int \overline{\rho}_b dr)$ (both are calculated by (6)) for average ion of this Al plasma are $\mu_e = -127.4928557$ eV and $Z^* = 4.1399487$, respectively, and these values are in good agreement with other typical theoretical results. Orbital energies of average atom obtained by (2) are shown in Table 1. In this table, mean orbital radii $\langle r \rangle$ are also shown, and these were all smaller than the ion-sphere radius a_{ion} though wave functions are solved under the boundary condition as shown in (2). For the case of comparatively high temperature, some mean orbital radii of bound electrons become larger than the a_{ion}, but such orbitals are not discard for calculating the bound electron density (see, (5)).

The radial distribution function $g_{ii}(r)$ obtained by (8) is shown in Figure 2. The coupling constant Γ of the plasma, which is defined in this paper as $\Gamma = (Z^*)^2/(a_{\text{ion}}T)$, is 1.2, so this Al plasma may be regarded as a strongly coupled plasma.

For calculation the photoabsorption cross section by (55) using DCA, the probability distributions $P_{\{\mathbf{q}\}}$ (see, (16)) must be estimated for congurations $\mathbf{q}$ as many as possible, and the normalization factor Z_G^{ion} is the sum of those distributions in order to satisfy the conservation of probability; that is,

$$Z_G^{\text{ion}} = \sum_{\{\mathbf{q}\}} P_{\{\mathbf{q}\}}. \tag{56}$$

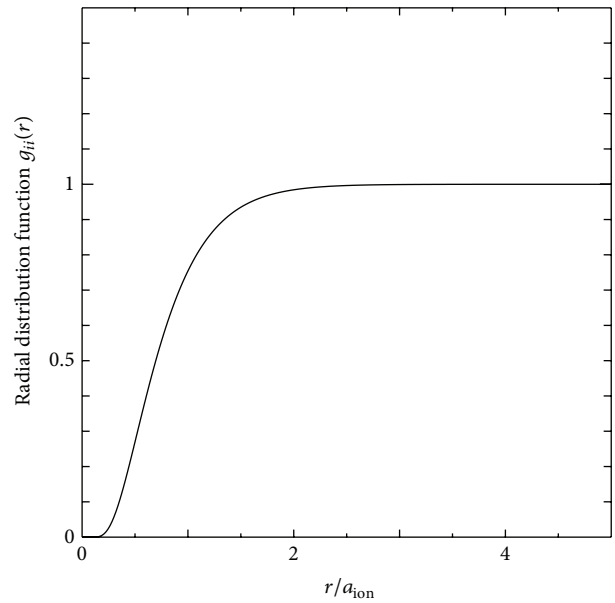

Figure 2: The radial distribution function $g_{ii}(r)$ of Al plasma (0.01 g/cm^3, 20 eV) obtained by HNC (see (8) and (9)). The coupling constant Γ is 1.2.

The summation is over all configurations used in (55), where the number of terms is usually huge even if we limit the maximum number of orbitals [13]. However, here we carried out the summation of (55) on two assumptions.

(I) The maximum principle quantum number is 8; namely, the electron configuration is described as follows:

$$(1s)^{q_1}(2s)^{q_2}(2p)^{q_3}(3s)^{q_4}(3p)^{q_5}(3d)^{q_6}\cdots(8\ell = 7)^{q_{36}}. \tag{57}$$

(II) The number of excited electrons from grand state is 3 or less.

For an Al ion, the total number of electron configurations on these assumptions is 703,236.

The total energy of an ion with the above assumed electron configuration cannot always be obtained because the ion is not isolated but is immersed in the plasma. Hence, it is regarded than an ion with such an electron configuration is unstable in the plasma and we omit this configuration from the summation of (55).

The number of stable electron configurations for this Al plasma was 288,737; the conservation of probability equation (16) was established by these 288,737 electron configurations. Table 2 shows the ten greatest probabilities obtained.

The population fraction W_Q of ions with charge state Q $(= Z_a - \sum_{i=1}^{36} q_i)$ is calculated using the probability $P_{\{\mathbf{q}\}}$ as follows:

$$W_Q = \sum_{\substack{q_1, q_2, q_3, \cdots \\ \sum q_i = Z_a - Q}} P_{\{\mathbf{q}\}}. \tag{58}$$

Figure 3 shows the charge state distribution of ions obtained for this Al plasma. In this Al plasma, there was no

Table 2: Probability distribution of electronic configuration $\{\mathbf{q}\}$ of ion in the Al plasma (0.01 g/cm^3, 20 eV) calculated by (22). Charge state Q means $Q = Z_a - \sum_{i=1}^{36} q_i$. The top 10 probabilities are shown in descending order starting from the highest probability.

Configuration	$\{\mathbf{q}\}$	$P_{\{\mathbf{q}\}}$	Charge state Q
$1s^2 2s^2 2p^5$	(2, 2, 5, 0, 0, 0, 0, ...)	0.297933	4
$1s^2 2s^2 2p^4$	(2, 2, 4, 0, 0, 0, 0, ...)	0.201386	5
$1\ s^2 2s^2 2p^6$	(2, 2, 6, 0, 0, 0, 0, ...)	0.030392	3
$1s^2 2s^1 2p^5$	(2, 1, 5, 0, 0, 0, 0, ...)	0.027722	5
$1s^2 2s^2 2p^4 3p^1$	(2, 2, 4, 0, 1, 0, 0, ...)	0.022315	4
$1s^2 2s^2 2p^4 3d^1$	(2, 2, 4, 0, 0, 1, 0, ...)	0.021047	4
$1s^2 2s^1 2p^6$	(2, 1, 6, 0, 0, 0, 0, ...)	0.015942	4
$1s^2 2s^2 2p^5 3d^1$	(2, 2, 5, 0, 0, 1, 0, ...)	0.014986	3
$1s^2 2s^2 2p^5 3p^1$	(2, 2, 5, 0, 1, 0, 0, ...)	0.014871	3
$1s^2 2s^2 2p^5 5f^1$	(2, 2, 5, 0, 0, 0, 1, ...)	0.011916	3

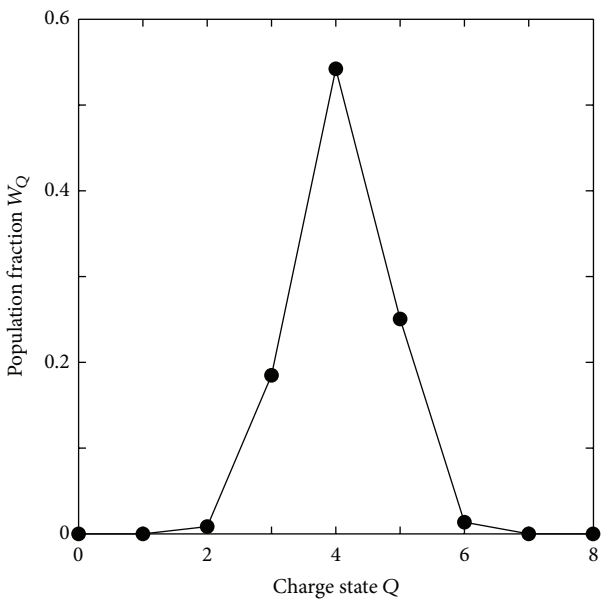

Figure 3: Charge state distribution W_Q of (58) for the Al plasma (ρ_{ion} = 0.01 g/cm^3, T = 20 eV). The average of charge state $\langle Q \rangle$ is 4.07952, although FTDFT in Section 2 gives this value as 4.1399487.

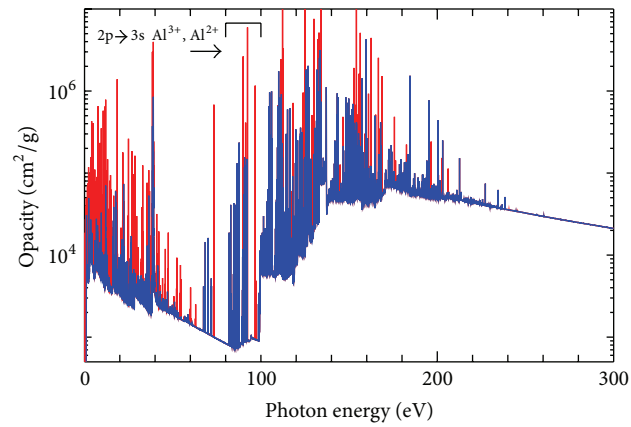

Figure 4: Red solid line: opacity equations (55) obtained by (50) and (54) for the Al plasma (ρ_{ion} = 0.01 g/cm^3, T = 20 eV). Blue solid line: opacity included contribution of autoionization resonance only (50). Both of the red and blue lines don't include Doppler width ans Stark width. 2p $\rightarrow$ 3s absorption lines of Al^{+2} and Al^{+3} are indicated in the figure.

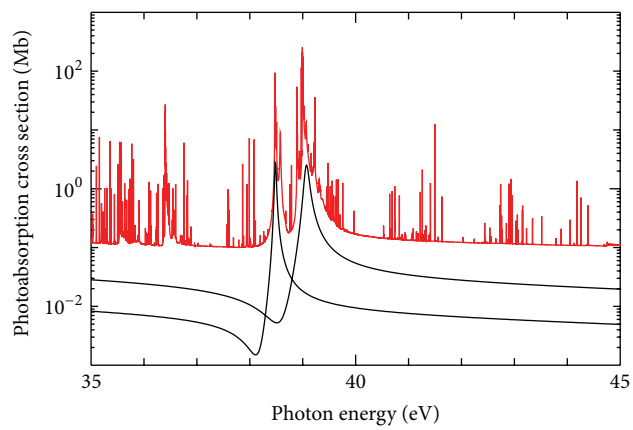

Figure 5: Opacity equations (55) included contribution of autoionization resonance only (50) for the Al plasma (ρ_{ion} = 0.01 g/cm^3, T = 20 eV). It is the same as the opacity shown by red line in Figure 4, but photon energy range is 35 eV–45 eV. Two black lines are Fano profiles; these mostly contributed the photoabsorption cross section with respect to the transition 2p $\rightarrow$ 3s of Al^{+3}.

ion of charge state $Q = 0$ (neutral atom) and population fraction of W_1 ($Q = 1$) is about 1.54×10^{-5} [1]. The average of charge state $\langle Q \rangle$ is 4.07952, about 1.5 percent less than $Z^*(= Z_a - \int \overline{\rho}_b dr)$ obtained by FTDFT (see, (5)).

The photoabsorption cross section (55) was calculated by selecting the top 500 probable electron configurations (from the total 288,737 configurations). In Figure 4, we show the opacity obtained by (50) and (54) for the Al plasma. In this result, the Doppler width was not considered and the profile of (54) was taken to be rectangle profile of width 4×10^{-4} eV. Figure 5 shows the absorption cross section for the photon energy range 35–45 eV. There are large two peaks in the vicinity of 38 eV; these are superposition of some Fano proles with respect to the transition 2p $\rightarrow$ 3s as shown in Figure 4, we show the two Fano profiles by black lines in Figure 5, which are most contributed to make that structure.

Figure 6 shows the opacity obtained by (50) including the Stark width (electron impact width:FWHM=0.4 eV [1]). Resonance points (see, (46)) and transitions of some Fano profiles (a–g in Figure 6) are shown in Table 3. In this table, two transitions for each profiles compete with each other as mentioned in Section 3.2. For example, profile "a" is identified as channel mixing of two processes b-b (2s $\rightarrow$ 2p) and b-f (3d $\rightarrow$ free) for an initial state ($1s^2 2s^2 2p^4 3d^1$) of Al^{4+}. In this case, b-f transition from 2p cannot occur because the incident photon energy is smaller than the threshold energy of 2d $\rightarrow$ free.

Figure 7 shows the opacity of ordinary b-b resonance by calculated by (54) including the Stark width (electron

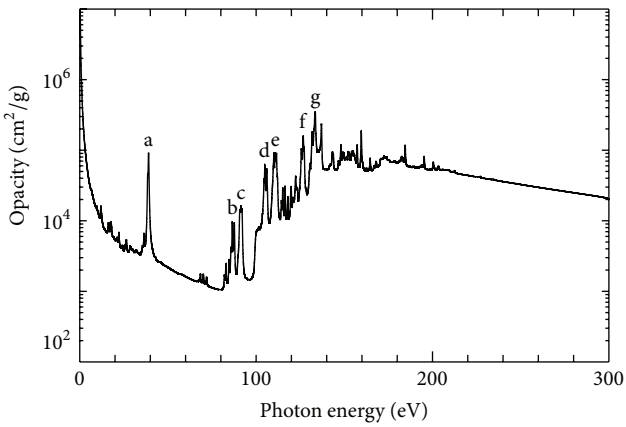

Figure 6: Opacity of Al plasma ($\rho_{\text{ion}} = 0.01\,\text{g/cm}^3$, $T = 20\,\text{eV}$) obtained by (55) without b-b resonance (see, (54)) but included Stark width. Spiking profiles are all Fano profiles, and symbols a–g indicate comparatively large Fano profiles.

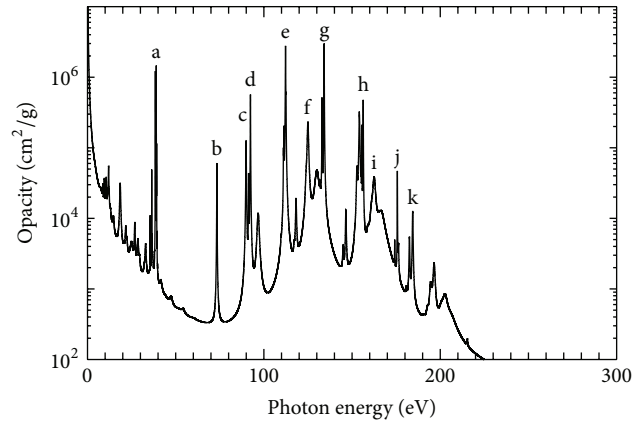

Figure 7: Opacity for b-b resonance of Al plasma ($\rho_{\text{ion}} = 0.01\,\text{g/cm}^3$, $T = 20\,\text{eV}$) obtained by (55) with (54), not including autoionization resonance. Spiking profiles are all b-b resonance profiles with Stark width.

Table 3: Assignment of lines a–g in Figure 6. Electronic configurations and two transitions with respect to autoionization resonance are shown for each line.

Symbol	Initial state	Transition
a	$Al^{4+} : 1s^2 2s^2 2p^4 3d^1$	$2s \rightarrow 2p, 3d \rightarrow$ free
b	$Al^{3+} : 1s^2 2s^2 2p^5 3[spd]^1$	$2p \rightarrow 3s, 3p \rightarrow$ free
c	$Al^{3+} : 1s^2 2s^2 2p^5 4[spf]^1$	$2p \rightarrow 3s, 4f \rightarrow$ free
d	$Al^{3+} : 1s^2 2s^2 2p^5 3[pd]^1$	$2p \rightarrow 3d, 3d \rightarrow$ free
e	$Al^{3+} : 1s^2 2s^2 2p^5 [4d4f5d5f]^1$	$2p \rightarrow 3d, 4, 5d \rightarrow$ free
f	$Al^{4+} : 1s^2 2s^2 2p^4 3[pd]^1$	$2p \rightarrow 3d, 3d \rightarrow$ free
g	$Al^{4+} : 1s^2 2s^2 2p^4 3[pd]^1$	$2p \rightarrow 3d, 3d \rightarrow$ free

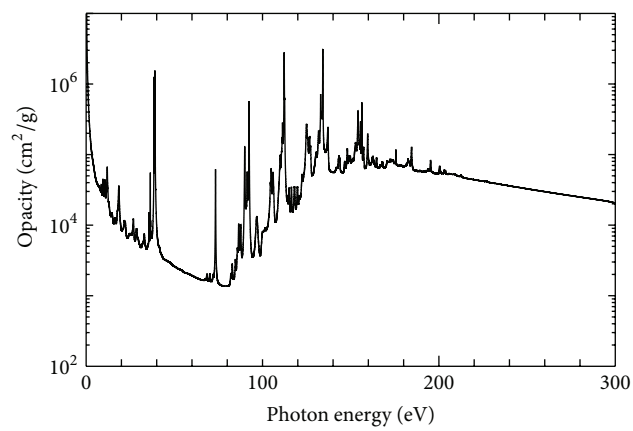

Figure 8: Opacity of Al plasma ($\rho_{\text{ion}} = 0.01\,\text{g/cm}^3$, $T = 20\,\text{eV}$) summed up b-f (Figure 6) and b-b (Figure 7) results.

Table 4: Assignment of lines a–k in Figure 7. Electronic configurations and transitions are shown for each line.

Symbol	Initial state	Transition
a	$Al^{4+} : 1s^2 2s^2 2p^5$	$2s \rightarrow 2p$
b	$Al^{3+} : 1s^2 2s^2 2p^6$	$2p \rightarrow 3s$
c	$Al^{3+} : 1s^2 2s^2 2p^6$	$2p \rightarrow 3d$
d	$Al^{4+} : 1s^2 2s^2 2p^5$	$2p \rightarrow 3s$
e	$Al^{4+} : 1s^2 2s^2 2p^5$	$2p \rightarrow 3d$
f	$Al^{5+} : 1s^2 2s^2 2p^4$	$2p \rightarrow 3s$
g	$Al^{4+} : 1s^2 2s^2 2p^5$	$2p \rightarrow 4d$
h	$Al^{5+} : 1s^2 2s^2 2p^4$	$2p \rightarrow 3d$
i	$Al^{5+} : 1s^2 2s^2 2p^4$	$2p \rightarrow 4d$
j	$Al^{5+} : 1s^2 2s^2 2p^4$	$2s \rightarrow 3p$
k	$Al^{5+} : 1s^2 2s^2 2p^4$	$2p \rightarrow 5d$

impact width). Symbols a–k in this figure show some major resonances; these resonance points and transition processes are shown in Table 4.

The opacity of Al plasma under consideration is the sum of two opacities equations (50) and (54), or the sum of Figure 6 and Figure 7; then its result is shown in Figure 8. The blue solid line in Figure 8 shows the same opacity but without the contribution from (54), showing several narrow autoionization resonance profiles and the dominant autoionization above 100 eV.

The transmission $F(\omega) = e^{-\rho\kappa(\omega)L}$ of the Al plasma is shown in Figure 9, where the path length L is chosen to be $L = 0.003$ cm [1] and the Stark width is considered by convolution of the obtained photoabsorption cross section and a Gaussian type profile. In the transmission, we considered Kramers cross section for free-free absorption, but we have not included the scattering cross section.

5. Conclusion

We propose a new model of calculating radiative opacity of hot dense plasmas in LTE using the detailed configuration accounting (DCA) including not only bb and bf contributions but also autoionization contributions. Electronic structures for ion with integer number of bound electrons, embedded in the plasma, are calculated by Kohn-Sham equation, and estimate the probability distribution of energies of such ions in the plasmas. The electrostatic potential surrounding an ion is determined by means of FTDFT [16]. The photoabsorption

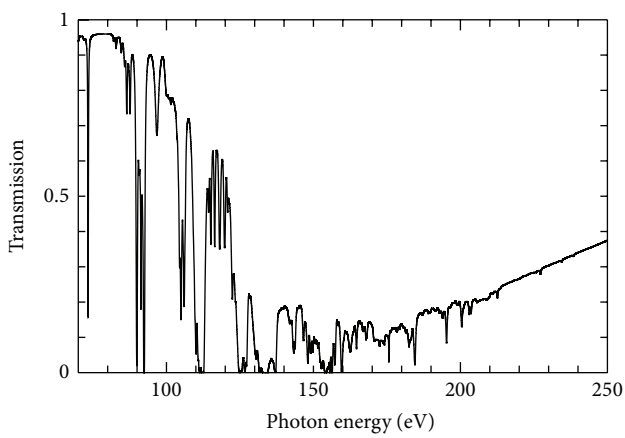

Figure 9: Transmission spectra obtained for Al plasma (ρ_{ion} = 0.01 g/cm^3, T = 20 eV). The Doppler width is considered by convolution of the cross section obtained and a Gaussian profile.

cross section of an ion with integer occupations is obtained by the previously derived formula by means of TDDFT [15], where Doppler and Stark width are both included.

In conclusion, we have calculated the opacity and transmission of an Al plasma (T = 20 eV, 0.01 g/cm^3) in the energy region 0–300 eV, but not considered the width caused of the unresolved transition array (UTA). The results are in good agreement with the experimental results of Winhart et al. [28] and theoretical results of Zeng et al. [1], in spite of the small number (500) of electron configurations used to calculate the photoabsorption. The Planck mean opacity and Rosseland mean opacity obtained were 28,348 cm^2/g and 4,279 cm^2/g, respectively. These mean opacities were calculated from the photoabsorption cross section obtained considering the Doppler width. The Rosseland mean opacity is very sensitive to the width of the line profile, so calculating this mean opacity is necessary to account for the autoionization resonance profile and other spectral widths. It is important to include the UTA width in our model so that width may be the most dominant in hot dense plasmas, and it is a subject for future analysis.

Conflict of Interests

The author declares that there is no conflict of interests regarding the publication of this paper.

References

[1] J. Zeng, J. Yuan, and Q. Lu, "Detailed-term-accounting-approximation calculations of the radiative opacity of laser-produced Al plasmas," *Physical Review E*, vol. 64, Article ID 066412, 2001.

[2] J. M. Bizau, C. Blancard, D. Cubaynes et al., "Experimental and theoretical studies of the photoionization cross section of Fe4+," *Physical Review A: Atomic, Molecular, and Optical Physics*, vol. 73, no. 2, Article ID 020707, 2006.

[3] A. Aguilar, J. D. Gillaspy, G. F. Gribakin et al., "Absolute photoionization cross sections for Xe4+, Xe5+, and Xe6+ near 13.5 nm: experiment and theory," *Physical Review A*, vol. 73, no. 3, Article ID 032717, 2006.

[4] F. Jin, J. Zeng, and J. Yuan, "Radiative opacities and configuration interaction effects of hot iron plasma using a detailed term accounting model," *Physical Review E*, vol. 68, Article ID 066401, 2003.

[5] W. R. Johnson, C. Guet, and G. F. Bertsch, "Optical properties of plasmas based on an average-atom model," *Journal of Quantitative Spectroscopy and Radiative Transfer*, vol. 99, no. 1–3, pp. 327–340, 2006.

[6] Z. Wu, J. Pang, and J. Yan, "Opacity calculations for high-Z plasma in non-local thermodynamic equilibrium," *Journal of Quantitative Spectroscopy & Radiative Transfer*, vol. 102, no. 3, pp. 402–408, 2006.

[7] A. Bar-Shalom, J. Oreg, and M. Klapisch, "EOSTA—an improved EOS quantum mechanical model in the STA opacity code," *Journal of Quantitative Spectroscopy and Radiative Transfer*, vol. 99, no. 1–3, pp. 35–54, 2006.

[8] D. S. J. Stein and A. Ron, "Average-atom models of line broadening in hot dense plasmas," *Physical Review A*, vol. 31, p. 446, 1985.

[9] B. F. Rozsnyai, "Collisional-radiative average-atom model for hot plasmas," *Physical Review E*, vol. 55, pp. 7507–7521, 1997.

[10] T. Blenski, A. Grimaldi, and F. Perrot, "Hartree-Fock statistical approach to atoms and photoabsorption in plasmas," *Physical Review E*, vol. 55, no. 5, pp. R4889–R4892, 1997.

[11] M. Das, M. K. Srivastava, and S. V. G. Menon, "Radiative opacity of low-Z plasma using screened hydrogenic model including l-splitting," *Journal of Quantitative Spectroscopy and Radiative Transfer*, vol. 113, no. 4, pp. 286–293, 2012.

[12] J. Pain and T. Blenski, "Self-consistent approach for the thermodynamics of ions in dense plasmas in the superconfiguration approximation," *Journal of Quantitative Spectroscopy and Radiative Transfer*, vol. 81, no. 1–4, pp. 355–369, 2003.

[13] A. Bar-Shalom, J. Oreg, W. H. Goldstein, D. Shvarts, and A. Zigler, "Super-transition-arrays: a model for the spectral analysis of hot, dense plasma," *Physical Review A*, vol. 40, no. 6, pp. 3183–3193, 1989.

[14] T. Blenski and K. Ishikawa, "Relation between the super-transition-array method in opacity calculations and the Hartree-Fock approximation at nonzero temperature," *Physical Review E*, vol. 51, no. 2, pp. 1602–1604, 1995.

[15] S. Kiyokawa, "Derivation of the Fano profile from time-dependent density-functional theory for local thermodynamic equilibrium plasmas," *Physical Review A*, vol. 75, Article ID 042501, 2007.

[16] S. Kiyokawa, "One-component plasmas with self-consistently determined core electrons," *Journal of the Physical Society of Japan*, vol. 64, no. 12, pp. 4708–4725, 1995.

[17] C. Blancard and G. Faussurier, "Equation of state and transport coefficients for dense plasmas," *Physical Review E*, vol. 69, no. 1, Article ID 016409, 2004.

[18] N. D. Mermin, "Thermal properties of the inhomogeneous electron gas," *Physical Review*, vol. 137, 1965.

[19] J. P. Perdew, R. G. Parr, M. Levy, and J. L. Balduz Jr., "Density-functional theory for fractional particle number: derivative discontinuities of the energy," *Physical Review Letters*, vol. 49, no. 23, pp. 1691–1694, 1982.

[20] R. Vuilleumier, M. Sprik, and A. Alavi, "Computation of electronic chemical potentials using free energy density functionals," *Journal of Molecular Structure: THEOCHEM*, vol. 506, pp. 343–353, 2000.

[21] K.-C. Ng, "Hypernetted chain solutions for the classical one−component plasma up to Γ=7000," *Chemical Physics*, vol. 61, p. 2680, 1974.

[22] A. Zangwill and P. Soven, "Density-functional approach to local-field effects in finite systems: Photoabsorption in the rare gases," *Physical Review A*, vol. 21, no. 5, pp. 1561–1572, 1980.

[23] M. Stott and E. Zaremba, "Linear-response theory within the density-functional formalism: application to atomic polarizabilities," *Physical Review A*, vol. 21, no. 1, p. 12, 1980.

[24] F. Grimaldi, A. Grimaldi-Lecourt, and M. W. C. Dharma-Wardana, "Time-dependent density-functional theory of light absorption in dense plasmas: application to iron plasma," *Physical Review A*, vol. 32, no. 2, pp. 1063–1071, 1985.

[25] E. Runge and E. K. U. Gross, "Density-functional theory for time-dependent systems," *Physical Review Letters*, vol. 52, pp. 997–1000, 1984.

[26] O. Ciricosta, S. M. Vinko, and H. K. Chung, "Direct measurements of the ionization potential depression in a dense plasma," *Physical Review Letters*, vol. 109, Article ID 065002, 2012.

[27] J. C. Slater, *Quantum Theory of Atomic Structure*, vol. 1, McGraw-Hill, New York, NY, USA, 1960.

[28] G. Winhart, K. Eidmann, C. A. Iglesias, and A. Bar-Shalom, "Measurements of extreme uv opacities in hot dense Al, Fe, and Ho," *Physical Review E*, vol. 53, no. 2, pp. R1332–R1335, 1996.